Conductive MOFs

International Edition: DOI: 10.1002/anie.201506219
German Edition: DOI: 10.1002/ange.201506219

Electrically Conductive Porous Metal–Organic Frameworks

Lei Sun[+], *Michael G. Campbell*[+], *and Mircea Dincă**

Keywords:
charge transport · conductivity · devices · metal–organic frameworks · porous materials

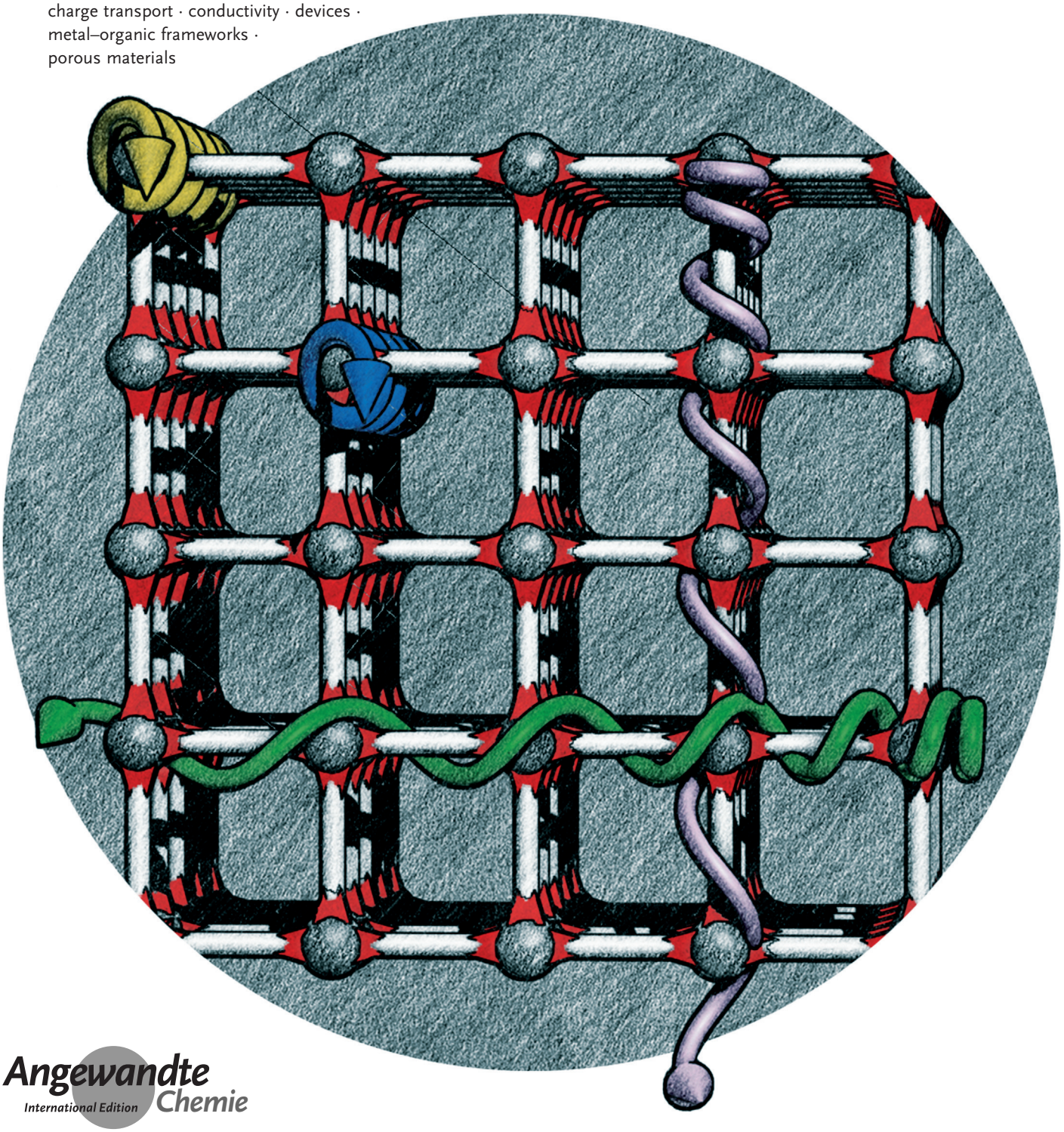

Owing to their outstanding structural, chemical, and functional diversity, metal–organic frameworks (MOFs) have attracted considerable attention over the last two decades in a variety of energy-related applications. Notably missing among these, until recently, were applications that required good charge transport coexisting with porosity and high surface area. Although most MOFs are electrical insulators, several materials in this class have recently demonstrated excellent electrical conductivity and high charge mobility. Herein we review the synthetic and electronic design strategies that have been employed thus far for producing frameworks with permanent porosity and long-range charge transport properties. In addition, key experiments that have been employed to demonstrate electrical transport, as well as selected applications for this subclass of MOFs, will be discussed.

From the Contents

1. Introduction

Metal–organic frameworks (MOFs) are a class of porous, high surface area materials that have been investigated for a myriad of applications, most prominent of which are gas separation[1] and storage.[2–4] Porous MOFs usually exhibit very low electrical conductivity, however, which limits their utility in a number of desirable technologies, such as fuel cells, supercapacitors, thermoelectrics, and resistive sensing.[5–11] The low electrical conductivity is a direct consequence of how these materials are typically constructed: hard metal ions are connected by redox-inactive organic ligands that bind via hard oxygen or nitrogen atoms.[12] Therefore, the vast majority of MOFs do not provide any low-energy pathway for charge transport, nor any free charge carriers, and behave as electrical insulators with conductivity lower than 10^{-10} S cm^{-1}. Only in the past five years have new approaches been realized that allow for the construction of MOFs that simultaneously exhibit both porosity and high charge mobility and/or electrical conductivity.[10,13,14] Herein, we survey the development of conductive MOFs to date, with a particular focus on the design principles that have been successfully used to engender conductivity. We restrict our scope to exclude the broader field of conductive coordination polymers that do not exhibit permanent porosity,[15] as well as frameworks that exhibit ion or proton conductivity,[16,17] as these categories of materials have been reviewed elsewhere.

2. General Design Principles and Concerns

Electrical conductivity (σ) is the key factor by which a conductive MOF is judged. Conductivity is dictated by the density (n) and mobility (μ) of electrons (e) and holes (h). Both high charge density and high charge mobility are thus needed to achieve high conductivity [Eq. (1)]:

$$\sigma = e(\mu_e n_e + \mu_h n_h) \quad (1)$$

High charge density requires that the material contains a high concentration of loosely bound charge carriers ($> 10^{15}$ cm^{-3}). These can be either free carriers, as in metallic conductors, or they can be thermally activated, as in semiconductors. Both the metal ions and the organic ligands of a MOF could be sources of charge carriers. The metal ions should have high-energy electrons or holes, for example, the unpaired electron of square-planar d^9 Cu^{II} centers or the minority-spin electron of high-spin octahedral d^6 Fe^{II} centers. The organic ligands should be either stable radicals, to provide unpaired electrons, or redox-active molecules to enable facile charge transfer between metal ions or nodes.

Band theory also points out important approaches to improve the charge density of a material, and the highly ordered crystal structures of MOFs warrant the application of band theory to understand their electronic structures. According to band theory, the energy levels in the material form continuous energy bands. In metallic conductors, bands are filled up to the Fermi level (E_F), which lies in the middle of a band. This band is called the conduction band and is not completely filled. Electrons in this band are all free charge carriers and, as a result, the charge density in a metallic conductor is typically higher than 10^{20} cm^{-3}, giving rise to high electrical conductivity (> 100 S cm^{-1}).[18]

In semiconductors and insulators, the Fermi level lies in a band gap between the valence band and the conduction band. At absolute zero, the valence band is completely filled, while the conduction band is completely empty. The energy difference between Fermi level and the valence band maximum (E_{VBM}) or the conduction band minimum (E_{CBM}) is called activation energy (E_a) [Eq. (2)]:

$$E_a = E_F - E_{VBM} \quad \text{or} \quad E_a = E_{CBM} - E_F \quad (2)$$

[*] L. Sun,[+] Dr. M. G. Campbell,[+] Prof. M. Dincă
Department of Chemistry
Massachusetts Institute of Technology
77 Massachusetts Avenue, Cambridge, MA 02139 (USA)
E-mail: mdinca@mit.edu
Homepage: http://web.mit.edu/dincalab
[+] These authors contributed equally to this work.

At a finite temperature, valence-band electrons are thermally promoted into the conduction band, leaving holes in the valence band. Both electrons and holes become free charge carriers. Charge density is therefore determined by the activation energy [Eq. (3)]:

$$n = n_0 \exp\left(-\frac{E_a}{kT}\right) \quad (3)$$

where n_0 is a prefactor, k is the Boltzmann constant, and T is absolute temperature. Clearly, the smaller the activation energy is, the larger the charge density is at a given temperature. In undoped (intrinsic) semiconductors, the Fermi level lies at the center of the band gap, thus a narrow band gap is preferred, which requires redox matching between the components of semiconductors. In doped (extrinsic) semiconductors, the dopant energy level shifts the Fermi level closer to the band edge of either the valence band or the conduction band, giving rise to p-type or n-type semiconductors with small activation energies.[19]

Charge mobility reflects the efficiency of charge transport. As for other materials, there are two main charge-transport regimes to consider for MOFs: hopping transport and band transport.[20] From a design perspective, both modes of transport require good spatial and energetic overlap between orbitals of appropriate symmetry; improving the charge transport pathway by increasing orbital overlap will increase charge mobility. In the hopping transport regime, charge carriers (i.e. electrons and/or holes) are localized at specific sites with discrete energy levels, and hop between neighboring sites. Charge mobility scales with the hopping probability (P), which is in turn governed by the spatial distance (R) and the energy difference (E) between neighboring hopping sites [Eq. (4)]:[21]

$$P = \exp\left(-\alpha R - \frac{E}{kT}\right) \quad (4)$$

where α is a constant that depends on the nature of hopping sites, and the other terms are defined as above.

In the band transport regime, charge carriers are delocalized, with effective masses (m^*) determined by the band curvature. Charge mobility is dictated by the effective mass of the charge carriers and the frequency of charge scattering events [Eq. (5)]:[18]

$$\mu = \frac{e\tau}{m^*} \quad (5)$$

where e is the elemental charge, and τ is the mean time between two charge-scattering events. A high density of charge-scattering sites, such as disorder, defects, impurities, or grain boundaries, will lead to a small τ and thus low mobility. Achieving high mobility also requires that charge carriers have small effective mass. Although the effective mass is affected by a complex set of factors including band dispersion, crystal lattice symmetry, and unit-cell parameters, an essential requirement that leads to a small effective mass is a well-dispersed band, which is fundamentally a result of good orbital overlap. Finally, owing to more facile charge delocalization, band transport naturally gives rise to higher charge mobility and typically to higher overall conductivity than hopping. Band transport should therefore be the ultimate goal when aiming for highest conductivity values when designing new electrically conductive MOFs.

Both hopping transport and band transport require low-energy charge-transport pathways; however, as discussed above, such pathways are absent in the vast majority of MOFs. To this end, there have been two general synthetic approaches towards providing charge-transport pathways in these materials: a "through-bond" approach, and a "through-space" approach.[22] In principle, both approaches can give rise to either hopping or band transport. The through-bond approach aims to promote charge transport via favorable spatial and energetic overlap of the metal and ligand orbitals involved in covalent bonding. The through-space approach enables charge transport via non-covalent interactions (such as π–π stacking) between electroactive fragments (i.e. molecular components with readily accessible redox couples, be it organic or inorganic) that are held in place by the metal–ligand bonds of the MOF. The permanent porosity of MOFs offers another variable for improving conductivity: the incorporation of guest molecules. The guest molecules can act as charge carriers themselves, as in the case of ionically conductive MOFs. Alternatively, redox-active guest molecules may act as charge dopants, thereby inducing free charge carriers within the MOF skeleton or walls through guest–framework charge-transfer interactions. Although effective, the use of guest molecules to improve conductivity in a given material inevitably reduces the porosity, limiting the materials' applicability in scenarios where high surface areas are desirable.

Herein, we discuss the electrically conductive MOFs reported to date, organized based on their idealized charge-transport pathways to provide intuitive design principles for

Lei Sun was born in 1988 in Changchun, China. He earned his B.S. at Nanjing University in 2011, with Prof. Jinglin Zuo on molecular conductors. He also worked on conductive coordination polymers with Prof. Kim R. Dunbar as an undergraduate research assistant at Texas A&M University, College Station. He is currently a graduate student at MIT with Prof. Mircea Dincă, working on electronic devices based on MOFs.

Michael G. Campbell was born in 1986 in Pennsylvania, and received his B.S. in 2008 from Loyola University, Maryland. He earned his Ph.D. in 2014 from Harvard University, where he worked on the chemistry of palladium(III) complexes with Prof. Tobias Ritter. He is currently a postdoctoral fellow at MIT with Prof. Mircea Dincă, working in the field of conductive MOFs.

those interested in the field. Critically, we note that the charge-transport mechanism that is targeted or "designed" into a particular MOF need not align with the transport mechanism that is in fact operative in the resulting material. Indeed, for most conductive MOFs reported to date, little if any experimental evidence exists addressing the nature of charge transport. Assigning hopping or band transport models to a given material may thus be premature; significant future work will be needed before the nature of charge transport in MOFs is understood.

3. Measurement Techniques

Electrical measurements are notoriously challenging because they depend not just on the intrinsic properties of the material being measured, but also on the materials used for device fabrication—electrical leads, contact pastes, substrates—and the quality of the device itself. Thus, before examining the known examples of electrically conductive MOFs, we discuss the techniques that have been used to measure the electrical conductivity and charge mobility of MOFs. We refer the interested reader to several more specialized Reviews for further theoretical and practical details of these techniques.[15,23–27]

3.1. Conductivity Measurements

By definition, characterization of electrical conductivity involves measuring electrical conductance (G), and length (l), and area (A) of the conduction channel [Eq. (6)]:

$$\sigma = G\frac{l}{A} = \frac{I}{V} \times \frac{l}{A} \tag{6}$$

Electrical conductance follows Ohm's law and is measured by taking the ratio between electrical current (I) and voltage (V), or by fitting a linear I–V curve. In most materials the I–V curve is linear, thus obeying Ohm's law, only when the current density is low, so the applied current or voltage should be as small as possible. I–V curves can be obtained by the two-probe method, four-probe method, or van der Pauw method (Figure 1).[15] The two-probe method measures the sum of resistances of the material, wires, and contacts, so this method requires the material to be significantly more resistive than the wires and contacts. The four-probe and van der Pauw methods eliminate the resistance of the contacts and wires, so they are suitable for materials with higher conductivity. The reported conductivity of most 3D MOFs is below 10^{-3} S cm^{-1}, giving rise to a resistance of more than 1 kΩ in a conduction channel. This is significantly larger than the typical resistance of contacts and wires (usually in the range of 1–10 Ω), such that the two-probe method is often sufficient to provide meaningful values of conductivity. However, more-recently developed layered MOFs exhibit electrical conductivity as high as 1580 S cm^{-1} (see below).[28] For these and any other materials with conductivity on the same order of magnitude as the electrical contacts, four-probe or van der Pauw methods should be employed to obtain meaningful results.

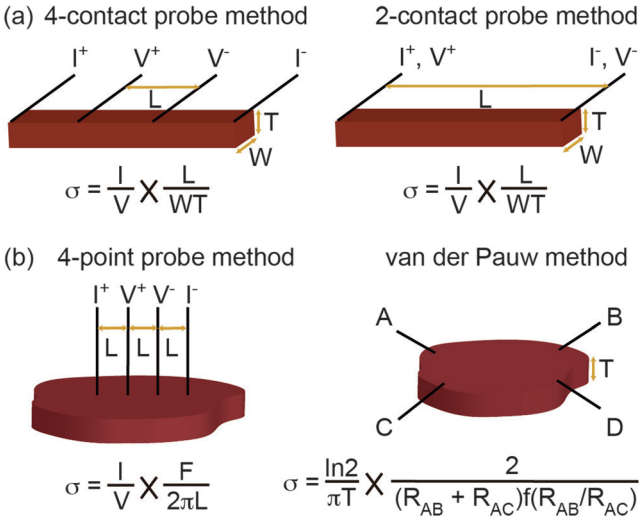

Figure 1. Techniques for measuring electrical conductivity of MOF samples, either as a) single crystals or pressed pellets, or b) thin films. I, V, L, W, and T represent current, voltage, length, width, and thickness, respectively. F is a correction factor. $R_{AB} = V_{CD}/I_{AB}$, $R_{AC} = V_{BD}/I_{AC}$. The function $f(R_{AB}/R_{AC})$ depends on the ratio between R_{AB} and R_{AC}. Both F and $f(R_{AB}/R_{AC})$ can be found in Ref. [23].

An important concern for electrical conductivity measurements is the physical form in which the MOF sample is measured. Pressed pellets, polycrystalline films, single-domain films, and single crystals may all be used and they naturally give different values. When comparing materials, it is also important to check, and preferably specify, what morphologies are being compared. For MOFs, most measurements so far have been performed on pressed pellets, prepared by compressing a powder under high pressure. Pressed pellets are readily accessible and easy to handle, but have drawbacks: 1) the high number of grain boundaries between crystallites prevents the study of intrinsic charge-transport properties and may contribute to reproducibility problems because of variations in the pelletization pressure or grain sizes, and 2) the random orientation of crystallites within the pellet masks any potential anisotropy of charge transport. Thus, the pellet or bulk conductivity is limited by the least conductive direction of the material and grain boundaries, both of which contribute to underestimated values for the intrinsic conductivity (i.e. the conductivity of a defect-free single crystal). An alternative means to obtain

Mircea Dincă (born 1980, in Făgăras, Romania), received a B.A. degree from Princeton University in 2003 and a PhD from UC Berkeley in 2008, working with Prof. Jeff Long. He started his independent career in 2010 after a postdoctoral stint with Prof. Dan Nocera. His group's research is focused on the synthesis and study of porous, crystalline extended solids as platforms for gas/vapor sorption, heterogeneous catalysis, and electronic applications.

bulk conductivity values is by evaluating the electrical properties of polycrystalline films. These are typically denser than pressed pellets and therefore show higher conductivity, but otherwise suffer from the same drawbacks as pellets. In contrast, single crystals and single-domain films have few grain boundaries, so they are suitable for studying intrinsic and anisotropic properties of charge transport. However, single crystals and single-domain films may be inaccessible or challenging to handle for some MOFs depending on factors including their crystallite size, air sensitivity, and mechanical strength. In addition, it can be difficult to accurately measure the conduction-channel length and area of single crystals owing to their irregular shape. In this case, only the order of magnitude of conductivity is meaningful. The commonly used techniques for measuring electrical conductivity of pressed pellets, films, and single crystals are summarized in Figure 1.

The environment is another key factor in evaluating and interpreting conductivity values for MOFs. The large surface area of these materials allows for significant interaction between the framework and the surrounding gas (e.g. oxygen or water vapor in air) or an adsorbed solvent. These guest molecules may, and often do, induce variations in conductivity. Finally, conductivity is affected by temperature and may also vary with exposure to radiation of various wavelengths, including visible light.

Given all of the above, it becomes clear that the ideal method to obtain intrinsic conductivity values, which is the norm by which conductive MOFs should be compared, is to perform four-probe measurements on single crystals (or van der Pauw measurements on single-domain films) in vacuum, at constant temperature, and in the dark. Obviously, these ideal conditions may not be feasible owing to various experimental limitations. However, when one or more of these conditions are not met, it is imperative that readers check the experimental details before interpreting or comparing reported conductivity values, and that researchers are accordingly careful about detailing their measurement conditions. We have made an effort herein to describe measurement conditions each time a conductivity value is cited, whenever such information is available.

3.2. Charge-Mobility Measurements

There are exceedingly few reports of charge-mobility measurements in MOFs. In a few examples, charge mobility was measured by time-resolved microwave conductivity (TRMC) techniques or in a field-effect transistor (FET). Although both methods rely on injecting a known and overwhelmingly large amount of charge carriers into a material and measuring the electrical conductivity, the results obtained from the two methods are not directly comparable and should not be used interchangeably. TRMC is an alternative current technique, whereas FET devices are typically evaluated under direct current. More significantly, TRMC reveals short-range (a few nm) charge-transport behavior under low electric field ($< 10\,V\,cm^{-1}$), while FET reveals long-range (tens of μm) charge-transport behavior under high electric field (10^4 to $10^5\,V\,cm^{-1}$).[26,29] The TRMC method is thus perhaps better fitted to describe intrinsic transport, whereas the FET method may be more indicative of transport in bulk, as would be expected for a device. Besides TRMC and FET, Hall-effect measurements, time-of-flight (TOF), and space-charge limited current (SCLC) methods are also useful for measuring charge mobility.[24,25] Clearly, because charge mobility is an important parameter for electrical devices, future work will need to place an increased focus on studies of charge mobility in MOFs. Although not trivial, these techniques are routinely used in organic electronics and should thus be readily accessible for those interested in this field.

3.3. Activation-Energy and Band-Gap Measurements

The activation energy is another important parameter for understanding the electrical properties of semiconductors. As discussed in Section 2, it reflects how easily charge carriers can be excited, and is dependent on the doping level. A low activation energy generally leads to a high charge density and hence high electrical conductivity. For semiconductors, the activation energy (E_a) is typically obtained by fitting temperature-dependent conductivity data to the Arrhenius equation [Eq. (7)]:

$$\sigma = \sigma_0 \exp\left(-\frac{E_a}{kT}\right) \tag{7}$$

where σ_0 is a prefactor. This formula requires the charge mobility to be constant in the temperature range used for the measurement.

It is common to use the activation energy to derive the fundamental band gap (E_g) by applying the formula $E_g = 2\,E_a$, where E_g is the energy difference between the valence band maximum and the conduction band minimum. However, care should be taken because this relationship is valid only when the semiconductor is intrinsic (undoped).[19] UV-Vis-NIR absorption measurements are also widely used to derive the fundamental band gap, but such an analysis is often not suitable for MOFs because the optical band gap and the fundamental band gap differ by a value equal to the exciton binding energy.[30] Most appropriately, the fundamental band gap should be measured directly by performing ultraviolet photoelectron spectroscopy (UPS) and inverse photoemission spectroscopy (IPES). These techniques measure the exact energy levels of the valence band maximum and the conduction band minimum, respectively.

4. Conductive MOFs: Experimental Approaches

4.1. The "Through-Bond" Approach to Charge Transport

A possible pathway for charge transport in MOFs is through the covalent linkages of extended coordination polymers within the porous framework. A wide variety of coordination polymers, such as 1D metal chain complexes,

have been reported to exhibit excellent conductivities.[15,31–33] Although these complexes are non-porous, and therefore fall outside the scope of this Review, their good electrical properties serve as strong encouragement that incorporation of such structural elements into porous MOFs is a promising strategy for accessing MOFs with high conductivity. In terms of MOF design, such an approach requires conjugated organic ligands, metal ions that contain loosely bound electrons, and relatively covalent bonding interactions between the metal ions and the organic ligands. For example, molecules and coordination polymers based on the metal bis(dithiolene) moiety are highly conductive,[34,35] and the covalency of the metal–sulfur bonds in these materials is likely important for charge transport.

In 2009, Takaishi et al. reported one of the first conductive MOFs, $Cu[Cu(pdt)_2]$ (pdt = 2,3-pyrazinedithiolate).[36] Its electrical conductivity is $6\times10^{-4}\,S\,cm^{-1}$ (300 K), and it exhibits a thermal activation energy of 0.193 eV. In $Cu[Cu(pdt)_2]$, Cu^{II} ions bridged by pdt ligands through the N atoms form square two-dimensional (2D) sheets (Figure 2b). The

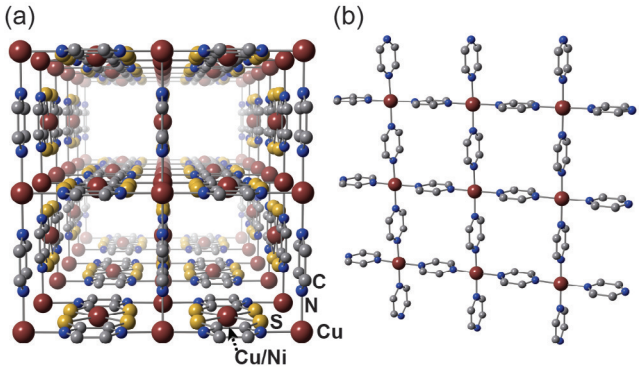

Figure 2. a) 3D structure of $Cu[Cu(pdt)_2]$ and $Cu[Ni(pdt)_2]$; b) View of a single Cu(pyrazine) 2D sheet in $Cu[Ni(pdt)_2]$, which is connected by Ni(dithiolene) units.

sheets are connected in the third dimension by redox-active copper bis(dithiolene) units to form a 3D framework (Figure 2a). Single-crystal X-ray diffraction and magnetic susceptibility confirmed both Cu atoms as divalent, as expected for their square-planar coordination environment. Adjacent pdt ligands are orthogonal to one another, and the shortest distance between two parallel pdt ligands is 6.82 Å. This distance is much longer than the van der Waals distance between pdt ligands, ruling out the possibility of through-space charge transport. Therefore, charge transport is likely through the [Cu(pyrazine)] 2D sheets via the copper bis(dithiolene) units, with the high-energy unpaired electron of d^9 Cu^{II} likely contributing to the relatively high conductivity of this MOF by increasing charge density. We note, however, that the charge-hopping formalism cannot be ruled out, because the redox active Cu dithiolene units are within optimal hopping distance of each other.

Although the crystal structure of $Cu[Cu(pdt)_2]$ indicates its porosity, it collapses upon desolvation. By replacing $Cu(pdt)_2^{2-}$ with $Ni(pdt)_2^{2-}$, Kobayashi et al. reported in 2010 an analogous MOF, $Cu[Ni(pdt)_2]$, which is permanently porous with a BET surface area of $385\,m^2\,g^{-1}$ (Figure 2a).[37] The conductivity of this MOF is only $1\times10^{-8}\,S\,cm^{-1}$ (film, two-probe, room temperature), however, which is more than four orders of magnitude lower than for $Cu[Cu(pdt)_2]$. A higher activation energy of 0.49 eV was also measured. We speculate that the low conductivity in $Cu[Ni(pdt)_2]$ may be rationalized by a lower charge density as a result of replacement of half of the d^9 Cu^{II} sites with d^8 Ni^{II} sites. The measured electrochemical potential of $[Ni(pdt)_2]^{2-/1-}$ is 0.257 V less negative than the value of $[Cu(pdt)_2]^{2-/1-}$; its weaker oxidizing power supports that the Ni^{II} center does not provide high-energy electrons as effective charge carriers. Upon exposing $Cu[Ni(pdt)_2]$ to I_2 vapor at 50 °C, its conductivity increases four orders of magnitude to a saturation conductivity of $1\times10^{-4}\,S\,cm^{-1}$, and the activation energy drops to 0.18 eV.[37] Weight analysis established that the I_2 loading is small, indicating that the charge transport is through the framework rather than through the I_2 guest molecules.[38,39] The increase in conductivity was ascribed to the partial oxidation of $[Ni(pdt)_2]^{2-}$ by I_2, which provides loosely bound unpaired electrons as charge carriers. These studies demonstrate the benefit of using redox-active building units, which may allow for improved electrical conductivity via doping.

Another strategy to realize through-bond charge transport is based on extended inorganic 1D chains or 2D sheets formed by the metal ions and the coordinating atoms of the organic ligands. These can be considered as dimensionally reduced versions of their bulk inorganic counterparts, such as metal oxides, metal pnictides, and metal chalcogenides. This strategy requires proper symmetry, spatial, and energy overlap of the orbitals of the metal ions and the coordinating atoms, the energy overlap may be inferred from the relative electronegativities of the atoms involved. For example, because the electronegativity values for transition metals are better matched with that of sulfur than that of oxygen (redox matching),[40] metal–organic chains or sheets connected through metal–sulfur bonds are expected to provide better charge transport pathways than structurally analogous metal–oxygen chains/sheets. Semiconducting coordination polymers based on metal–sulfur chains have been reported,[41,42] and this idea is also applicable to MOFs.

This concept of redox matching has been illustrated in the M_2(DOBDC) frameworks (M = Mg, Mn, Fe, Co, Ni, Cu, Zn, $DOBDC^{4-}$ = 2,5-dihydroxybenzene-1,4-dicarboxylate). Also known as the MOF-74 or CPO-27 family of MOFs, these are a set of structurally analogous, permanently porous materials that have one-dimensional structural building units (SBUs) with infinite $(\text{-M-O-})_\infty$ chains connected through the phenoxide groups of DOBDC (Figure 3).[43–49] Surmising that replacement of the phenoxide O atoms in DOBDC with S atoms would lead to MOF-74-type MOFs containing $(\text{-Mn-S-})_\infty$ SBUs instead of $(\text{-Mn-O-})_\infty$, Sun et al. treated Mn^{2+} with 2,5-disulfhydrylbenzene-1,4-dicarboxylic acid (H_4DSBDC), and isolated Mn_2(DSBDC).[50] This material indeed has 1D $(\text{-Mn-S-})_\infty$ chains and remains permanently porous, exhibiting a BET surface area of $978\,m^2\,g^{-1}$ (Figure 3). TRMC and TOF measurements showed that the intrinsic charge mobility of

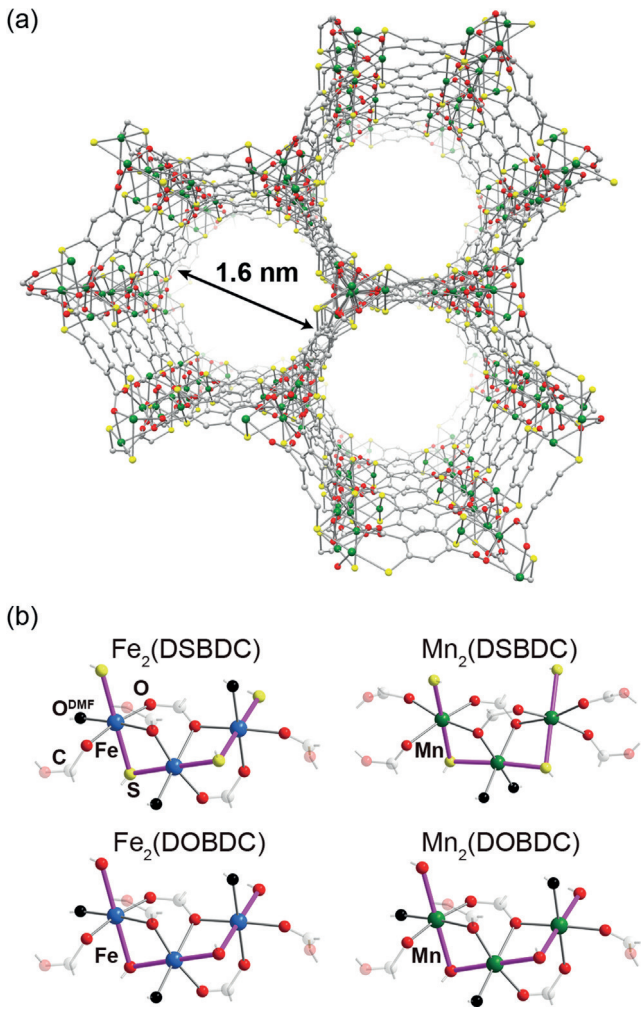

Figure 3. a) Structure of M_2(DOBDC) and M_2(DSBDC) MOFs, showing 1D pores; b) Infinite M–S and M–O chains; (M = Fe, Mn).

the activated Mn_2(DSBDC) is 0.01 $cm^2 V^{-1} s^{-1}$. This value is comparable to the charge mobility found in organic semiconductors measured by the same techniques.[26]

Although Mn_2(DSBDC) has a relatively high charge mobility, its charge density is expectedly very low because the ligand $DSBDC^{4-}$ is not a radical, and the d^5 Mn^{II} ions do not contribute minority-spin electrons.[51] Accordingly, the conductivity of both DMF-coordinated Mn_2(DSBDC) (2.5×10^{-12} S cm^{-1}, pressed pellet, two-probe, 297 K) and Mn_2(DOBDC) (3.9×10^{-13} S cm^{-1}, pressed-pellet, two-probe, 297 K) is very low. However, replacing d^5 Mn^{II} by d^6 Fe^{II} centers introduces high energy, loosely bound minority-spin carriers,[51] such that DMF-coordinated Fe_2(DSBDC) and Fe_2(DOBDC) (Figure 3b) exhibit conductivity of 3.9×10^{-6} S cm^{-1} (pressed pellet, two-probe, 297 K) and 3.2×10^{-7} S cm^{-1} (pressed pellet, two-probe, 297 K), respectively.[52] The addition of a single minority-spin carrier thus induces a remarkable increase in conductivity by six orders of magnitude. Although these materials conceptually fall in the "through-bond" formalism, band-structure calculations show that their valence and conduction bands are narrow (dispersion of < 100 meV), indicating that charge transport is better described by hopping. However, whereas Fe d orbitals dominate the valence band in Fe_2(DOBDC), such that holes likely hop between Fe^{II} centers with little contribution from bridging O atoms, both Fe and S orbitals feature prominently in the valence band of Fe_2(DSBDC), with holes likely using both and likely hopping more easily through the $(\text{-Fe-S-})_\infty$ chains. Notwithstanding, the minority-spin electron of high spin Fe^{II} is a key factor that leads to relatively high electrical conductivity of Fe_2(DSBDC) and Fe_2(DOBDC), and provides important insight for designing other materials in this class.

The benefit of using Fe^{II} is also reflected in Fe(1,2,3-triazolate)$_2$, a material reported by Gándara et al. in 2012.[53] In this MOF, Fe^{II} and 1,2,3-triazolate form a 3D porous network wherein charges likely hop between Fe^{II} centers, as inferred from the band-structure calculation of a 1D Fe(1,2,3-triazolate) coordination polymer (Figure 4).[54] The short Fe–Fe distances in Fe(1,2,3-triazolate)$_2$ should result in a high charge-hopping probability, and the measured conductivity is 7.7×10^{-5} S cm^{-1} (pressed pellet, four-probe, room temperature). It is noteworthy that among seven structurally analogous MOFs featuring Mg^{II}, Mn^{II}, Fe^{II}, Co^{II}, Cu^{II}, Zn^{II},[53] and Cd^{II},[55] Fe(1,2,3-triazolate)$_2$ is the only one for which electrical conductivity data has been reported. We note, however, that the small Fe–Fe distance also implies low-spin Fe^{II} centers, which do not contain unpaired electrons. More work will be needed to understand why Fe(1,2,3-triazolate)$_2$ displays a relatively high electrical conductivity.

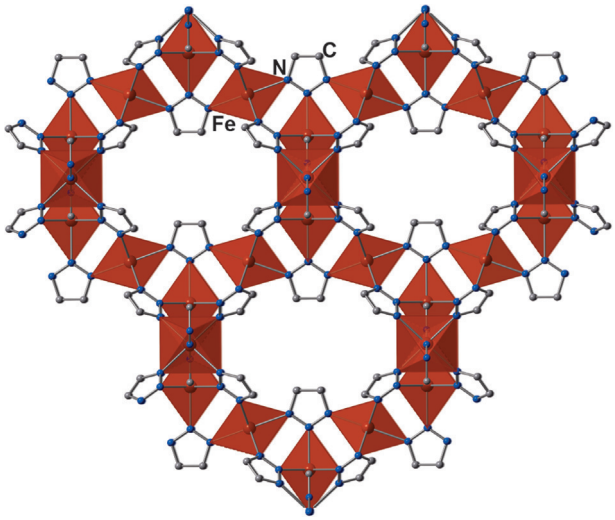

Figure 4. The structure of Fe(1,2,3-triazolate)$_2$, showing a continuous network of covalent Fe–N bonds.

Guest molecules can also act as bridges between SBUs to induce through-bond transport. In 2014, Talin et al. reported an intriguing example of this strategy.[56] By soaking the MOF $Cu_3(BTC)_2$ (HKUST-1, BTC^{3-} = benzene-1,3,5-tricarboxylate) in a saturated dichloromethane solution of TCNQ (7,7,8,8-tetracyanoquinodimethane), the conductivity can be tuned from 10^{-8} S cm^{-1} (film, four-probe) for the pristine MOF to 0.07 S cm^{-1} for a product with approximately one

TCNQ molecule per MOF pore by controlling the soaking time. Calculations suggest that the TCNQ molecules closely bind to two open Cu sites of the activated MOF, forming new charge transport pathways (Figure 5). Redox matching and orbital overlap between the framework and the guest TCNQ are again critical to induce efficient charge transport.[57–59] The

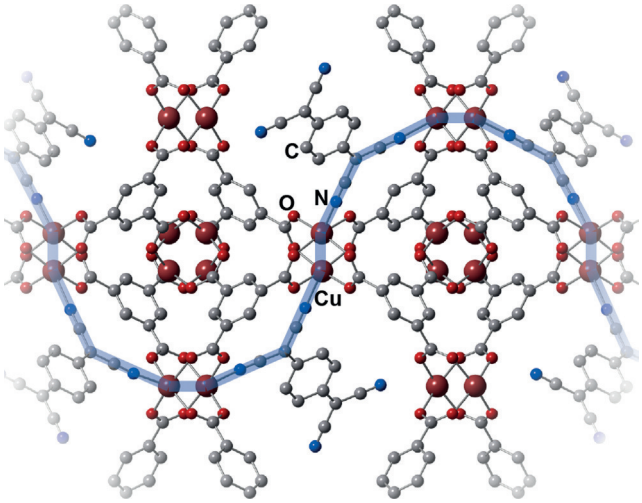

Figure 5. Predicted structure of TCNQ-adsorbed $Cu_3(BTC)_2$, with a covalent charge-transport pathway via Cu–TCNQ linkages highlighted in blue.

computed density of states (DOS) of the TCNQ-infiltrated $Cu_3(BTC)_2$ indicates close proximity between the valence-band maximum of $Cu_3(BTC)_2$ and the LUMO of TCNQ, giving rise to a very small activation energy of 0.041 eV. As a result, partial charge transfer of 0.3–0.4 e^- that creates loosely bound charge carriers occurs between the framework and the TCNQ molecules, as confirmed by Raman spectroscopy. The positive sign of the Seebeck coefficient measured for TCNQ-infiltrate $Cu_3(BTC)_2$ ($S = 375\ \mu V\,K^{-1}$ at room temperature)[58] confirmed holes as the majority charge carriers. Illustrative of the negative effects of guest incorporation on porosity, TCNQ insertion turns $Cu_3(BTC)_2$ from an insulator into a conductor, but also causes a significant reduction in the BET surface area from $1844 \pm 4\ m^2 g^{-1}$ for pristine $Cu_3(BTC)_2$ to $214 \pm 0.5\ m^2 g^{-1}$, consistent with pore occlusion by TCNQ guests.

Common to the examples discussed in this section is that the nature of the metal ions plays a key role in through-bond charge transport. Loosely bound electrons are critical for high conductivity in $Cu[Cu(pdt)_2]$, I_2-doped $Cu[Ni(pdt)_2]$, Fe_2(DSBDC), and Fe_2(DOBDC). This is an important and potentially useful concept, but more systematic studies are required to understand the contribution of metal ions to electrical conductivity from both experimental and theoretical perspectives. Future studies may inquire whether Fe^{II} is unique in promoting good conductivity, or whether other transition-metal ions with unevenly occupied d levels could fulfill the same role, for instance. More generally, we anticipate a higher prominence of metal ions with loosely bound electrons, such as square-planar Cu^{II} and octahedral high-spin Fe^{II} centers, and of redox-active organic ligands in the design of conductive MOFs. On a practical note, it may be expected that materials containing metal ions, such as high-spin Fe^{II}, are less stable under ambient conditions. However, such limitations could be circumvented by various processing techniques (such as the use of impermeable coatings); additionally, the observation of robust atmospheric stability for Fe(1,2,3-triazolate)$_2$ demonstrates that the development of conductive MOFs based on Fe^{II} does not necessarily impose practical limitations.

Charge transfer between guest molecules and metal ions or organic ligands is also a promising method for creating both charge-transport pathways and high charge density, as observed for TCNQ-infiltrated $Cu_3(BTC)_2$. Perhaps more so than in the case of MOFs with intrinsic conductivity, computational methods will become instrumental for screening host–guest pairs that can give rise to conductivity through guest insertion/intercalation. Indeed, computational studies have recently identified 45 additional MOFs that should become conductive upon TCNQ infiltration.[60] Because the through-bond charge transport strategy is amenable to reticular synthesis, rigorous inspection of existing MOFs may yield additional examples that could become conductive with minimal modification, as was the case for MOF-74.

4.2. The "Through-Space" Approach to Charge Transport

Inspired by molecular and polymeric organic conductors and semiconductors, such as TTF–TCNQ (TTF = tetrathiafulvalene)[61] and polythiophene,[62,63] the through-space approach has also been used to design conductive MOFs. This approach aims to use non-covalent interactions, such as π–π stacking between organic ligands, to create an extended charge-transport pathway using a rigid MOF structure that enforces close packing and sufficient orbital overlap between the adjacent ligands.[64] Ideally, this approach can give rise to band-like transport, as in TTF–TCNQ itself and other organic metals. Stable organic radicals are the best candidates for ligands because they provide free charge carriers, thereby improving charge density. A large body of literature exists on the use of this approach to design conductive coordination polymers or molecular conductors,[65,66] many of which display conductivity values in excess of 1 $S\,cm^{-1}$.[67–71] To our knowledge, however, none of these exhibit permanent porosity.

The first examples of porous and conductive 3D MOFs designed for through-space transport are a class of TTF-based materials reported by Narayan et al. in 2012, followed by Park et al. in 2015: M_2(TTFTB) (M = Mn, Co, Zn, and Cd; $TTFTB^{4-}$ = tetrathiafulvalene tetrabenzoate).[72,73] All four of these MOFs are isostructural, with TTF moieties forming π–π stacked 1D helical columns with relatively short S···S interactions between neighboring TTF molecules running parallel to infinite metal carboxylate SBUs (Figure 6). They exhibit BET surface areas between 470 and 540 $m^2\,mmol^{-1}$. DFT calculations show that p_z orbitals on the sulfur atoms and the central carbon atoms of the TTF moieties dominate the valence band of M_2(TTFTB). Close contacts between these orbitals on neighboring molecules give rise to some of the

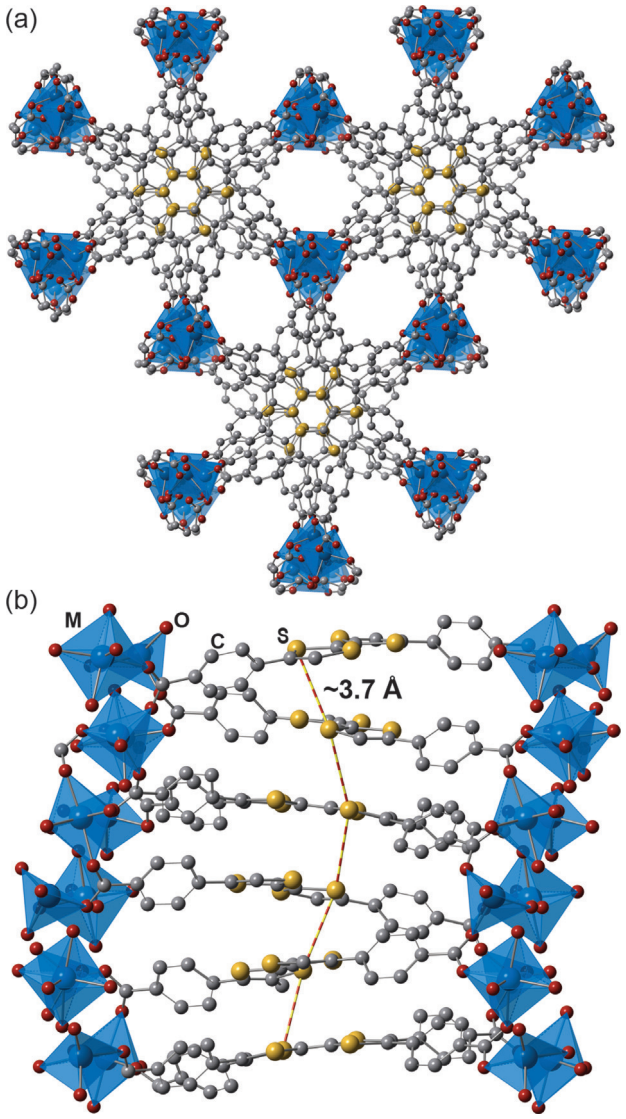

Figure 6. a) Structure of M_2(TTFTB) MOFs (M = Mn, Co, Zn, Cd); b) Side view of a helical TTF stack, showing the shortest intermolecular S···S contacts.

widest bands observed in MOFs, with a valence-band dispersion of 400 meV. In perfect single crystals, such a wide dispersion may be expected to give rise to band-like transport, which would result in high charge mobility. This is corroborated experimentally by TRMC and TOF measurements, which give an intrinsic charge mobility of 0.2 $cm^2V^{-1}s^{-1}$ for Zn_2(TTFTB).

In M_2(TTFTB), partial oxidation of the TTF groups to radical cations occurs even in the as-synthesized materials. This oxidation improves the charge density and leads to single-crystal conductivity values ranging from approximately 10^{-6} Scm^{-1} for Zn_2(TTFTB) and Co_2(TTFTB) to 10^{-5} Scm^{-1} for Mn_2(TTFTB), and 10^{-4} Scm^{-1} for Cd_2(TTFTB) (room temperature, single crystal, two-probe). The gradual increase in conductivity is correlated with a concomitant increase in the ionic radii of the metal cations. Because the metal carboxylate chains are not expected to contribute to charge transport in these materials, the positive correlation between cation radius and conductivity has been associated instead with the gradual decrease in the S···S distance between neighboring TTF moieties. Indeed, the S···S distance decreases from approximately 3.76 Å in Zn_2(TTFTB) and Co_2(TTFTB) to 3.65 Å in Cd_2(TTFTB), leading to improved orbital overlap and higher conductivity in Cd_2(TTFTB). Tuning charge transport using side chains is a well-studied topic in the field of organic conductors/semiconductors,[74] and these results show that the same strategy is also suitable for MOFs.

Panda et al. also targeted π–π stacking interactions to construct a series of 2D layered In^{III} isophthalate MOFs.[75] FET devices made from these materials showed no measurable charge mobility for a MOF that lacked π–π stacking interactions, whereas a drop-cast polycrystalline film of a structurally related material that featured π–π stacking between the 2D layers exhibited a charge carrier mobility of 4.6×10^{-3} $cm^2V^{-1}s^{-1}$ (Figure 7).

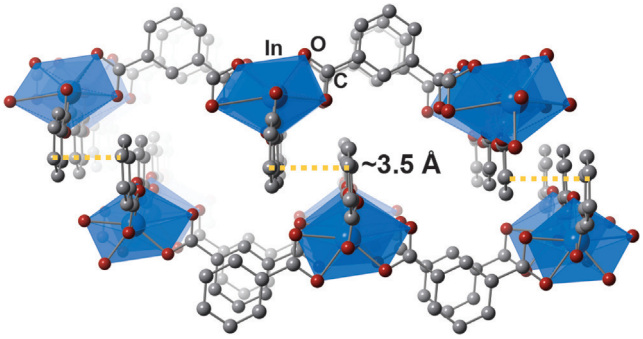

Figure 7. A layered In^{III} MOF in which increased π–π stacking between 2D layers leads directly to increased charge mobility.

The examples reported to date demonstrate that through-space charge transport in MOFs gives rise to charge mobility that is comparable with organic semiconductors (10^{-5}–10 $cm^2V^{-1}s^{-1}$). This is not surprising, especially for the M_2(TTFTB) MOFs, as the TTF stacks mimic the structure of charge-transfer salts. In addition, the M_2(TTFTB) MOFs demonstrate that organic radicals are beneficial to conductivity, a widely used strategy in molecular conductors. The incorporation of stable organic radicals is therefore a promising approach to design electrically conductive MOFs, and we expect that this strategy will be employed more widely in the near future. The In^{III} isophthalate MOF also highlights an especially interesting strategy that potentially involves both intra-sheet through-bond charge transport and inter-sheet through-space charge transport. A combination of these design principles is a promising and potentially very fruitful strategy for generating a wide variety of conductive MOFs. Finally, we note that the work on the In^{III} MOFs is a rare example of using MOFs to fabricate transistors, a strategy that will become important for more in-depth as well as applied studies of conductive MOFs.

4.3. 2D π-Conjugated MOFs

A special case of the "through-bond" approach to conductive MOFs is a family of planar 2D MOFs reminiscent of graphite. Although the area of porous, crystalline 2D polymers has been dominated by covalent organic frameworks (COFs), these generally lack good conjugation pathways in the 2D plane and accordingly are not ideal for electronic applications.[76–79] Structurally related 2D MOFs, in which the connection between organic linkers is typically a single metal ion (i.e. single metal ion SBU), have recently emerged as a promising alternative to COFs, especially with respect to electrical conductivity. The "through-bond" approach for these 2D MOFs is in the form of extended 2D π-conjugation.[80] Materials synthesized using this approach are the most conductive MOFs known. Theoretical calculations of monolayers of these materials reveal widely dispersed valence and conduction bands, indicating band transport and thus high charge mobility within the 2D sheets.

All reported materials in this class so far exhibit stacked honeycomb lattices and are made from benzene- or triphenylene-derived ligands with *ortho*-disubstituted N, O, or S donor atoms that define square-planar coordination environments with a variety of late-transition-metal nodes (Figure 8a). Each of the ligands is expected to be oxidized to achieve charge balance with the M^{2+} centers (Figure 8a, inset).[81] Ligand oxidation is likely critical for increasing the charge density and implicitly the conductivity of these materials. The hexagonal pores defined by triphenylene-based lattices are on the order of around 2 nm, although the stacking mode of the 2D sheets can vary in a manner similar to what is found in COFs (Figure 8b). In some cases, the sheets exhibit an eclipsed or slipped-parallel stacking structure, giving extended 1D pores; in other cases, the sheets stack in a staggered fashion and define smaller 1D pores. While there has been no reported example of control over eclipsed versus staggered stacking modes, an empirical trend suggests that 2D lattices made from metal–N or metal–O linkages tend to exhibit eclipsed or slipped-parallel structures, while S donor ligands are more likely to give staggered structures. Clearly, although the intra-sheet transport is expected to dominate the electrical properties of these materials, the stacking arrangement affects electrical transport between the 2D sheets, such that determining, and ideally controlling, the stacking geometry should be an important goal in this area.

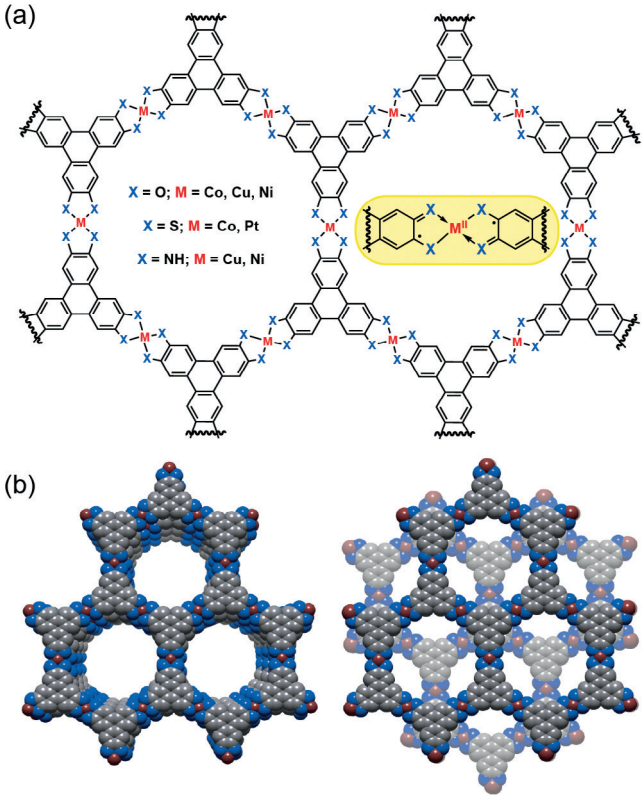

Figure 8. a) A portion of the infinite structure of hexagonal 2D MOFs based on triphenylene-derived ligands. The inset shows the oxidized radical anion form of the ligands, expected to be found in neutral frameworks with M^{2+} ions; b) Eclipsed and staggered packing modes observed for bulk materials based on stacking of 2D MOF sheets.

In 2012 Hmadeh et al. reported a series of metal catecholate frameworks, made by reaction of hexahydroxytriphenylene (H_6HHTP) with Co^{II} or Ni^{II} salts, which were shown to contain extended 2D sheets layered between molecular metal HHTP complexes (Figure 8; X = O; M = Co, Ni).[82] The structures of the Co and Ni 2D catecholate MOFs were established by X-ray crystallography and high-resolution transmission electron microscopy (HR-TEM). Both the Co- and Ni-based MOFs display permanent porosity, with BET surface areas of 490 and 425 $m^2 g^{-1}$, respectively. Although the electrical properties of the Ni and Co materials were not reported, single crystals of a related material synthesized from Cu^{II} and H_6HHTP exhibit a conductivity of 0.2 $S cm^{-1}$ (four-probe) at room temperature. However, powder X-ray diffraction (PXRD) analysis showed that the Cu–HHTP material is not isostructural with the Co- and Ni-based MOFs, and the structure was not assigned.

Several examples of metal dithiolene 2D MOFs have also been reported, based on either benzenehexathiol (H_6BHT) or hexathiotriphenylene (H_6HTTP). The first example of this family of MOFs was reported by Kambe et al. in 2013, who isolated $Ni_3(BHT)_2$ from H_6BHT and $Ni(OAc)_2$ (Figure 9a).[83] The bulk material consists of staggered honeycomb layers, although single-layer nanosheets can also be obtained by synthesizing the material at a liquid–liquid interface. A four-probe (van der Pauw) measurement on a microflake of $Ni_3(BHT)_2$ revealed an impressive conductivity of 160 $S cm^{-1}$ (Figure 9b).[84] Experimental studies also showed that the doping level affects the activation energy and the conductivity in this material. Pal et al. reported an analogous $Pd_3(BHT)_2$ structure in 2015, which exhibited a significantly lower room-temperature conductivity of 2.8×10^{-2} $S cm^{-1}$ (pressed pellet, four-probe).[85] In 2015, Huang et al. also reported the corresponding $Cu_3(BHT)_2$ material, which displays a record room-temperature conductivity of 1580 $S cm^{-1}$ (thin film, four-probe). FET measurements indicate ambipolar behavior, with charge mobilities of 99 and 116 $cm^2 V^{-1} s^{-1}$ for holes and electrons, respectively.[28]

In 2014 Cui et al. reported a related 2D MOF prepared from H_6HTTP and $PtCl_2$, which also displays a staggered

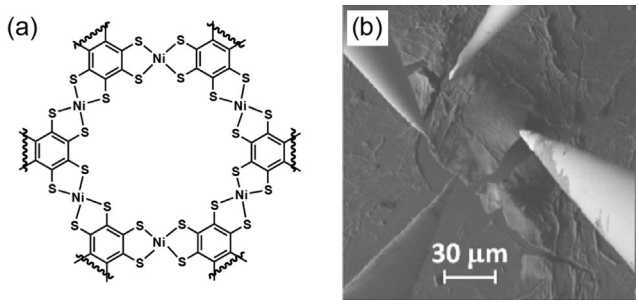

Figure 9. a) A portion of the infinite structure of a 2D Ni dithiolene MOF, synthesized by a liquid–liquid interface method; b) SEM image of a four-probe conductivity measurement of a microflake sample (image reproduced with permission from Ref. [84], copyright 2014 American Chemical Society).

stacking of 2D sheets (Figure 8; X = S; M = Pt).[86] The as-synthesized framework was anionic, with charge-balancing Na^+ cations, suggesting that the ligands were not oxidized sufficiently to afford a neutral framework. However, the anionic MOF could be oxidized to a neutral material with I_2. Upon evacuation, the neutral $Pt_3(HTTP)_2$ framework exhibits a BET surface area of 391 $m^2 g^{-1}$. The bulk conductivity (pressed pellet, two-probe) of both the as-synthesized and the I_2-doped samples was found to be on the order of 10^{-6} $S cm^{-1}$ at room temperature. This conductivity is much lower than those observed for materials in this class; measurements of single sheets or flakes of these materials could reveal whether the low conductivity is due to grain boundaries in the polycrystalline pellet or is an intrinsic property of the Pt MOFs. We also note that analogous MOFs made from Co^{II} with both H_6BHT and H_6HTTP as well as from Ni^{II} with H_6HTTP have been reported. They can be used, neat, as hydrogen-evolution electrocatalysts, and are thus likely conductive as well, but their conductivity has not been reported yet.[87,88]

Conductive 2D MOFs made from nitrogen-based ligands were the latest addition to this class. In 2014, Sheberla et al. reported that reaction of $NiCl_2$ with hexaaminotriphenylene (H_6HATP) in ammoniacal water leads to the isolation of $Ni_3(HITP)_2$ (HITP = hexaiminotriphenylene; Figure 8; X = NH; M = Ni), in which 2D honeycomb sheets stack in a slipped-parallel arrangement.[89] Polycrystalline films of $Ni_3(HITP)_2$ grown on a quartz substrate displayed a conductivity of 40 $S cm^{-1}$ (four-probe, van der Pauw) at room temperature, while pellets of the same material displayed a bulk conductivity of 2 $S cm^{-1}$ (two-probe). The isostructural material made from Cu^{II}, $Cu_3(HITP)_2$ (Figure 8; X = NH, M = Cu), displayed similar electrical properties, with a room temperature bulk conductivity of 0.2 $S cm^{-1}$ (two-probe). Significantly, the large bulk conductivity of HITP-based materials enabled the first application of MOFs in chemiresistive sensing: devices fabricated from $Cu_3(HITP)_2$ function as reversible and quantitative electrically resistive sensors for ammonia vapor.[90–91] Interestingly, preliminary experiments also demonstrated that the chemiresistive response can be altered by choice of metal node, $Ni_3(HITP)_2$ being unresponsive to ammonia. Although the sources of this differential behavior are not currently known, these studies highlight the utility of 2D conductive MOFs in the production of tunable functional materials, such as chemical sensors.

The emergence of the 2D π-conjugated frameworks has brought MOFs into the range of conductivity values that can enable real-life devices and applications. The first examples of electrocatalysis and resistive sensing, two of the more obvious applications, have already appeared and demonstrate very promising results. Much remains to be explored in these two areas, but additional work is imminent in other applications, such as electrical energy storage and thermoelectrics. A surge of theoretical work has also indicated that these materials may be of fundamental interest for evaluating exotic electronic states, such as half-metallicity[92] and topological insulator behavior.[93,94] While applications in both devices and condensed-matter physics are both appealing and encouraging, they all rely on much needed synthetic advances in this area. Systematically probing the influence of the metal ion, the ligand donor atom, the lattice geometry, and the doping level are just a few of the immediate structural and electronic factors that must be addressed. Likewise, reliable and general synthetic procedures that provide facile access to single- or few-layer sheets with large domain size will need to be developed if the exciting physical properties predicted by theory are to be experimentally tested.

5. Outlook

The field of electrically conductive MOFs has seen tremendous growth in the past several years and has yielded a variety of two- and three-dimensional MOFs with high charge mobility and/or electrical conductivity. Relevant data for the conductive MOFs reported to date is summarized in Table 1. (Note added in proof: a 2,5-dihydroxybenzoquinone-based MOF ($(NBu_4)_2Fe^{III}_2(dhbq)_3$, $\sigma = 0.16$ $S cm^{-1}$, pressed pellet, two-probe)[95] and an anthracene-based MOF (NNU-27, $\sigma = 1.3 \times 10^{-3}$ $S cm^{-1}$, single crystal, two-probe)[96] with high electrical conductivity have recently been reported. The physical properties of these two MOFs are also listed in Table 1.) Both "through-bond" and "through-space" strategies have enabled high charge mobility in MOFs, and we have begun to develop a better understanding of the approaches that can give rise to good charge transport through appropriate orbital interactions. The strategy of improving charge density by using metal ions and organic ligands with loosely bound electrons has also been established, and provides a key design principle for future work. However, a unified, fundamental understanding of conductivity in MOFs is still lacking in most cases, and significant experimental and theoretical future work will be needed to elucidate the mechanisms of charge transport in conductive MOFs.

The data in Table 1 makes clear that, even for the conductive MOFs reported so far, there is still a great deal that remains unknown. Furthermore, there are reports of MOF-based electrocatalytic, electrochromic, and photovoltaic devices,[97–99] in which charge transport most likely occurs via redox hopping, but measurements of these MOFs'

Table 1: Summary of data for conductive MOFs reported to date.

Compound Formula	Conductivity[a,b] [S cm^{-1}]	Charge Mobility[b] [cm^2 V^{-1} s^{-1}]	Activation Energy[c] [eV]	BET Surface Area[d]
Mn_2(DSBDC)[50,52]	2.5×10^{-12} (pellet, 2-probe)[g,i]	0.01,[k] 0.02[l] (TRMC/TOF)	0.81 (320–420 K)[e,j]	232 m^2 g^{-1}[j]
Mn_2(DOBDC)[52]	3.9×10^{-13} (pellet, 2-probe)[g,i]	*N.R.*[f]	0.54 (210–420 K)[e,j]	287 m^2·g^{-1}[j]
Mn_2(TTFTB)[73]	8.6×10^{-5} (crystal, 2-probe)[h]	*N.R.*	*N.R.*	594 m^2 g^{-1} 470 m^2 mmol^{-1}
Fe_2(DSBDC)[52]	3.9×10^{-6} (pellet, 2-probe)[g,i]	*N.R.*	0.28 (200–420 K)[e,j]	54 m^2 g^{-1}[j]
Fe_2(DOBDC)[52]	3.2×10^{-7} S cm^{-1} (pellet, 2-probe)[g,i]	*N.R.*	0.38 (200–420 K)[e,j]	241 m^2 g^{-1}[j]
Fe(1,2,3-triazolate)$_2$[53]	7.7×10^{-5} (pellet, 4-probe)[e]	*N.R.*	*N.R.*	450 m^2 g^{-1}
$(NBu_4)_2Fe_2$(dhbq)$_3$[95]	0.16 (pellet, 2-probe)[g]	*N.R.*	0.11 (70–300 K)[g]	*N.R.*
$Na_{0.9}(NBu_4)_{1.8}Fe_2$(dhbq)$_3$[95]	6.2×10^{-3} (pellet, 2-probe)[g]	*N.R.*	0.18 (70–300 K)[g]	*N.R.*
Co_2(TTFTB)[73]	1.5×10^{-5} (crystal, 2-probe)[h]	*N.R.*	*N.R.*	665 m^2 g^{-1} 531 m^2 mmol^{-1}
Ni_3(HITP)$_2$[88]	2 (pellet, 2-probe)[h] 40 (film, van der Pauw)[e]	*N.R.*	*N.R.*	*N.R.*
Ni_3(BHT)$_2$[83,84]	0.15 (pellet, 2-probe)[e,m] 2.8 (microflake, van der Pauw)[e,m] 160 (microflake, van der Pauw)[e,n]	*N.R.*	0.026[e,m] 0.010[e,n]	*N.R.*
Cu_3(HITP)$_2$[89]	0.2 (pellet, 2-probe)[h]	*N.R.*	*N.R.*	*N.R.*
Cu_3(HHTP)$_2$[82]	0.2 (crystal, 4-probe)	*N.R.*	*N.R.*	*N.R.*
Cu_3(BHT)$_2$[28]	1580 (film, 4-probe)[e]	99 (hole, FET) 116 (electron, FET)	0.00206 (300 K) 0.00012 (40 K)[e]	*N.R.*
Cu[Cu(pdt)$_2$][36]	6×10^{-4} (*N.R.*)	*N.R.*	0.193 (200–400 K)	*N.R.*
Cu[Ni(pdt)$_2$][37]	1×10^{-8} (film, 2-probe)[g]	*N.R.*	0.49 (film, 2-probe)[g]	385 m^2 g^{-1}
Cu[Ni(pdt)$_2$] (I_2-doped)[37]	1×10^{-4} (film, 2-probe)[o]	*N.R.*	0.18 (film, 2-probe)[g]	*N.R.*
TCNQ@Cu_3(BTC)$_2$[56]	0.07 (film, 4-probe)	*N.R.*	0.041 (125–300 K)	214 m^2 g^{-1}
Zn_2(TTFTB)[72,73]	4.0×10^{-6} (crystal, 2-probe)[h]	0.2 (TRMC/TOF)	*N.R.*	662 m^2 g^{-1} 537 m^2 mmol^{-1}
NNU-27[96]	1.3×10^{-3} (crystal, 2-probe)	*N.R.*	*N.R.*	*N.R.*
Pd_3(BHT)$_2$[85]	2.8×10^{-2} (film, 4-probe)	*N.R.*	*N.R.*	*N.R.*
Cd_2(TTFTB)[73]	2.9×10^{-4} (crystal, 2-probe)[h]	*N.R.*	*N.R.*	559 m^2 g^{-1} 521 m^2 mmol^{-1}
[In(isophthalate)$_2$]$^-$[75]	*N.R.*	4.6×10^{-3} (FET)[h]	*N.R.*	*N.R.*
Pt_3(HTTP)$_2$[86]	10^{-6} (pellet, 2-probe)[p]	*N.R.*	*N.R.*	391 m^2 g^{-1}

[a] Measured at room temperature. [b] Measurement method given in parentheses. [c] Temperature range used to determine activation energy given in parentheses. [d] As determined from the measured 77 K N_2 adsorption isotherm. [e] Measured in vacuum. [f] *N.R.* = not reported. [g] Measured in N_2 or Ar atmosphere. [h] Measured in ambient conditions. [i] Measured for M_2(DEBDC)(DMF)$_2$·*x*DMF (M = Mn, Fe; E = S, O). [j] Measured for M_2(DEBDC)(DMF)$_2$ (M = Mn, Fe; E = S, O). [k] Measured for activated Mn_2(DSBDC). [l] Measured for methanol-exchanged Mn_2(DSBDC). [m] Measured for $Na_{3/4}[Ni_3(BHT)_2]$. [n] Measured for neutral Ni_3(BHT)$_2$. [o] Measured in a flow of N_2 and I_2 vapor (N_2 flow rate 75 mL min^{-1}, I_2 flow rate 1.5 μmol min^{-1}). [p] Conductivity of as-synthesized, activated, and I_2 treated Pt_3(HTTP)$_2$ are all approximately 10^{-6} S cm^{-1}.

conductivity have not yet been reported. Indeed, critical metrics, such as charge mobility or activation energy, remain unknown for many established conductive MOFs, although these fundamental properties are important for semiconductor applications. Table 1 also highlights a lack of consistency regarding the measurement techniques and the experimental conditions employed for electrical measurements; we encourage researchers to pursue more rigorous and thorough measurements in future work. As discussed for several of the examples described above, theoretical calculations have also played a key role in understanding and predicting the electronic properties of these materials.[100,101] Although the large unit cells of many MOFs make ab initio, plane-wave calculations costly, we urge experimentalists to work with theoreticians when possible, as theoretical work on the electronic structure of MOFs will be critical as the field moves forward.

Finally, the development of MOFs whose conductivity rivals that of graphite, such as the 2D MOFs described in Section 4.3, has enabled the fabrication of the first MOF-based electrical or electrochemical devices that function in the absence of other additives. Although still rare, demonstrating the utility of MOFs in such devices is equally crucial for the development of the field, as this will attract scientists and engineers with broader interests to join these efforts. Given the rapid developments in synthetic, theoretical, and applied work in the last few years, we are confident that the field of conductive MOFs will continue to grow dramatically, and we hope that the strategies outlined herein will pave the way for the development of a new generation of MOF-based functional devices.

Acknowledgements

We gratefully acknowledge funding for various aspects of fundamental and applied conductive MOF research in our group from the Department of Energy (DOE) through the Center for Excitonics, an Energy Frontier Research Center funded by the DOE Office of Science, Office of Basic Energy

Sciences (Award DE-SC0001088), and through a Young Investigator Award to M.D. from the DOE Office of Science, Office of Basic Energy Sciences (Award DE-SC0006937). M.D. also thanks 3M, the Sloan Foundation, and the Research Corporation for Science Advancement for non-tenured faculty awards, and the Dreyfus Foundation for a postdoctoral fellowship in support of M.G.C.

How to cite: *Angew. Chem. Int. Ed.* **2016**, *55*, 3566–3579
Angew. Chem. **2016**, *128*, 3628–3642

[1] J.-R. Li, J. Sculley, H.-C. Zhou, *Chem. Rev.* **2012**, *112*, 869–932.
[2] K. Sumida, D. L. Rogow, J. A. Mason, T. M. McDonald, E. D. Bloch, Z. R. Herm, T.-H. Bae, J. R. Long, *Chem. Rev.* **2012**, *112*, 724–781.
[3] M. P. Suh, H. J. Park, T. K. Prasad, D.-W. Lim, *Chem. Rev.* **2012**, *112*, 782–835.
[4] H. Wu, Q. Gong, D. H. Olson, J. Li, *Chem. Rev.* **2012**, *112*, 836–868.
[5] N. P. Brandon, D. J. Brett, *Philos. Trans. R. Soc. A* **2006**, *364*, 147–159.
[6] P. Simon, Y. Gogotsi, *Nat. Mater.* **2008**, *7*, 845–854.
[7] M. D. Allendorf, A. Schwartzberg, V. Stavila, A. A. Talin, *Chem. Eur. J.* **2011**, *17*, 11372–11388.
[8] L. E. Kreno, K. Leong, O. K. Farha, M. Allendorf, R. P. Van Duyne, J. T. Hupp, *Chem. Rev.* **2012**, *112*, 1105–1125.
[9] O. Bubnova, X. Crispin, *Energy Environ. Sci.* **2012**, *5*, 9345.
[10] V. Stavila, A. A. Talin, M. D. Allendorf, *Chem. Soc. Rev.* **2014**, *43*, 5994–6010.
[11] L. Borchardt, M. Oschatz, S. Kaskel, *Mater. Horiz.* **2014**, *1*, 157–168.
[12] M. A. Nasalevich, M. van der Veen, F. Kapteijn, J. Gascon, *CrystEngComm* **2014**, *16*, 4919.
[13] D. M. D′Alessandro, J. R. R. Kanga, J. S. Caddy, *Aust. J. Chem.* **2011**, *64*, 718–722.
[14] C. H. Hendon, D. Tiana, A. Walsh, *Phys. Chem. Chem. Phys.* **2012**, *14*, 13120.
[15] G. Givaja, P. Amo-Ochoa, C. J. Gómez-García, F. Zamora, *Chem. Soc. Rev.* **2012**, *41*, 115–147.
[16] S. Horike, D. Umeyama, S. Kitagawa, *Acc. Chem. Res.* **2013**, *46*, 2376–2384.
[17] P. Ramaswamy, N. E. Wong, G. K. H. Shimizu, *Chem. Soc. Rev.* **2014**, *43*, 5913–5932.
[18] G. Grosso, G. P. Parravicini in *Solid State Physics*, 2nd ed. (Eds.: G. Grosso, G. P. Parravicini), Academic Press, Amsterdam, **2014**, pp. 483–528.
[19] G. Grosso, G. P. Parravicini in *Solid State Physics*, 2nd ed. (Eds.: G. Grosso, G. P. Parravicini), Academic Press, Amsterdam, **2014**, pp. 577–608.
[20] P. Stallinga, *Adv. Mater.* **2011**, *23*, 3356–3362.
[21] N. F. Mott, *Philos. Mag.* **1969**, *19*, 835–852.
[22] R. Hoffmann, *Acc. Chem. Res.* **1971**, *4*, 1–9.
[23] D. K. Schroder, *Semiconductor Material and Device Characterization*, Wiley, Hoboken, **2005**, pp. 1–59.
[24] S. Tiwari, N. C. Greenham, *Opt. Quantum Electron.* **2009**, *41*, 69–89.
[25] A. Kokil, K. Yang, J. Kumar, *J. Polym. Sci. Part B* **2012**, *50*, 1130–1144.
[26] A. Saeki, Y. Koizumi, T. Aida, S. Seki, *Acc. Chem. Res.* **2012**, *45*, 1193–1202.
[27] S. Roth, D. Carroll, *One-Dimensional Metals*, Wiley-VCH, Weinheim, **2014**, pp. 113–151.
[28] X. Huang, P. Sheng, Z. Tu, F. Zhang, J. Wang, H. Geng, Y. Zou, C.-A. Di, Y. Yi, Y. Sun et al., *Nat. Commun.* **2015**, *6*, 1–8.
[29] A. Saeki, S. Seki, T. Sunagawa, K. Ushida, S. Tagawa, *Philos. Mag.* **2006**, *86*, 1261–1276.
[30] J.-L. Bredas, *Mater. Horiz.* **2014**, *1*, 17–19.
[31] T. W. Thomas, A. E. Underhill, *Chem. Soc. Rev.* **1972**, *1*, 99–120.
[32] J. K. Bera, K. R. Dunbar, *Angew. Chem. Int. Ed.* **2002**, *41*, 4453–4457; *Angew. Chem.* **2002**, *114*, 4633–4637.
[33] M. G. Campbell, D. C. Powers, J. Raynaud, M. J. Graham, P. Xie, E. Lee, T. Ritter, *Nat. Chem.* **2011**, *3*, 949–953.
[34] J. R. Reynolds, J. C. W. Chien, C. P. Lillya, *Macromolecules* **1987**, *20*, 1184–1191.
[35] Y. Sun, P. Sheng, C. Di, F. Jiao, W. Xu, D. Qiu, D. Zhu, *Adv. Mater.* **2012**, *24*, 932–937.
[36] S. Takaishi, M. Hosoda, T. Kajiwara, H. Miyasaka, M. Yamashita, Y. Nakanishi, Y. Kitagawa, K. Yamaguchi, A. Kobayashi, H. Kitagawa, *Inorg. Chem.* **2009**, *48*, 9048–9050.
[37] Y. Kobayashi, B. Jacobs, M. D. Allendorf, J. R. Long, *Chem. Mater.* **2010**, *22*, 4120–4122.
[38] Z. Hao, G. Yang, X. Song, M. Zhu, X. Meng, S. Zhao, S. Song, H. Zhang, *J. Mater. Chem. A* **2014**, *2*, 237–244.
[39] S. H. Chae, H.-C. Kim, Y. S. Lee, S. Huh, S.-J. Kim, Y. Kim, S. J. Lee, *Cryst. Growth Des.* **2015**, *15*, 268–277.
[40] B. J. Holliday, T. M. Swager, *Chem. Commun.* **2005**, 23.
[41] D. L. Turner, T. P. Vaid, P. W. Stephens, K. H. Stone, A. G. DiPasquale, A. L. Rheingold, *J. Am. Chem. Soc.* **2008**, *130*, 14–15.
[42] D. L. Turner, K. H. Stone, P. W. Stephens, A. Walsh, M. P. Singh, T. P. Vaid, *Inorg. Chem.* **2012**, *51*, 370–376.
[43] N. L. Rosi, J. Kim, M. Eddaoudi, B. Chen, M. O′Keeffe, O. M. Yaghi, *J. Am. Chem. Soc.* **2005**, *127*, 1504–1518.
[44] P. D. C. Dietzel, Y. Morita, R. Blom, H. Fjellvåg, *Angew. Chem. Int. Ed.* **2005**, *44*, 6354–6358; *Angew. Chem.* **2005**, *117*, 6512–6516.
[45] P. D. C. Dietzel, B. Panella, M. Hirscher, R. Blom, H. Fjellvåg, *Chem. Commun.* **2006**, 959.
[46] P. D. C. Dietzel, R. Blom, H. Fjellvåg, *Eur. J. Inorg. Chem.* **2008**, 3624–3632.
[47] W. Zhou, H. Wu, T. Yildirim, *J. Am. Chem. Soc.* **2008**, *130*, 15268–15269.
[48] E. D. Bloch, L. J. Murray, W. L. Queen, S. Chavan, S. N. Maximoff, J. P. Bigi, R. Krishna, V. K. Peterson, F. Grandjean, G. J. Long et al., *J. Am. Chem. Soc.* **2011**, *133*, 14814–14822.
[49] R. Sanz, F. Martínez, G. Orcajo, L. Wojtas, D. Briones, *Dalton Trans.* **2013**, *42*, 2392–2398.
[50] L. Sun, T. Miyakai, S. Seki, M. Dincă, *J. Am. Chem. Soc.* **2013**, *135*, 8185–8188.
[51] Q. Zhang, B. Li, L. Chen, *Inorg. Chem.* **2013**, *52*, 9356–9362.
[52] L. Sun, C. H. Hendon, M. A. Minier, A. Walsh, M. Dincă, *J. Am. Chem. Soc.* **2015**, *137*, 6164–6167.
[53] F. Gándara, F. J. Uribe-Romo, D. K. Britt, H. Furukawa, L. Lei, R. Cheng, X. Duan, M. O′Keeffe, O. M. Yaghi, *Chem. Eur. J.* **2012**, *18*, 10595–10601.
[54] D. Tiana, C. H. Hendon, A. Walsh, T. P. Vaid, *Phys. Chem. Chem. Phys.* **2014**, *16*, 14463.
[55] X.-H. Zhou, Y.-H. Peng, X.-D. Du, J.-L. Zuo, X.-Z. You, *CrystEngComm* **2009**, *11*, 1964.
[56] A. A. Talin, A. Centrone, A. C. Ford, M. E. Foster, V. Stavila, P. Haney, R. A. Kinney, V. Szalai, F. El Gabaly, H. P. Yoon et al., *Science* **2014**, *343*, 66–69.
[57] M. D. Allendorf, M. E. Foster, F. Léonard, V. Stavila, P. L. Feng, F. P. Doty, K. Leong, E. Y. Ma, S. R. Johnston, A. A. Talin, *J. Phys. Chem. Lett.* **2015**, *6*, 1182–1195.
[58] K. J. Erickson, F. Léonard, V. Stavila, M. E. Foster, C. D. Spataru, R. E. Jones, B. M. Foley, P. E. Hopkins, M. D. Allendorf, A. A. Talin, *Adv. Mater.* **2015**, *27*, 3453–3459.
[59] C. H. Hendon, A. Walsh, *Chem. Sci.* **2015**, *6*, 3674–3683.
[60] X. Nie, A. Kulkarni, D. S. Sholl, *J. Phys. Chem. Lett.* **2015**, *6*, 1586–1591.

[61] J. Ferraris, D. O. Cowan, V. T. Walatka, J. H. Perlstein, *J. Am. Chem. Soc.* **1973**, *95*, 948 – 949.
[62] A. Tsumura, H. Koezuka, T. Ando, *Appl. Phys. Lett.* **1986**, *49*, 1210.
[63] H. Sirringhaus, P. J. Brown, R. H. Friend, M. M. Nielsen, K. Bechgaard, B. Langeveld-Voss, A. Spiering, R. A. Janssen, E. W. Meijer, P. Herwig, *Nature* **1999**, *401*, 685 – 688.
[64] H. Dong, X. Fu, J. Liu, Z. Wang, W. Hu, *Adv. Mater.* **2013**, *25*, 6158 – 6183.
[65] G. Saito, Y. Yoshida in *Topics in Current Chemistry*, Springer, Berlin, Heidelberg, **2011**, pp. 67 – 126.
[66] K. P. Goetz, D. Vermeulen, M. E. Payne, C. Kloc, L. E. McNeil, O. D. Jurchescu, *J. Mater. Chem. C* **2014**, *2*, 3065 – 3076.
[67] R. A. Heintz, H. Zhao, X. Ouyang, G. Grandinetti, J. Cowen, K. R. Dunbar, *Inorg. Chem.* **1999**, *38*, 144 – 156.
[68] C. Avendano, Z. Zhang, A. Ota, H. Zhao, K. R. Dunbar, *Angew. Chem. Int. Ed.* **2011**, *50*, 6543 – 6547; *Angew. Chem.* **2011**, *123*, 6673 – 6677.
[69] M. Ballesteros-Rivas, A. Ota, E. Reinheimer, A. Prosvirin, J. Valdés-Martinez, K. R. Dunbar, *Angew. Chem. Int. Ed.* **2011**, *50*, 9703 – 9707; *Angew. Chem.* **2011**, *123*, 9877 – 9881.
[70] Z. Zhang, H. Zhao, H. Kojima, T. Mori, K. R. Dunbar, *Chem. Eur. J.* **2013**, *19*, 3348 – 3357.
[71] F. Gándara, N. Snejko, A. de Andrés, J. R. Fernandez, J. C. Gómez-Sal, E. Gutierrez-Puebla, A. Monge, *RSC Adv.* **2012**, *2*, 949 – 955.
[72] T. C. Narayan, T. Miyakai, S. Seki, M. Dincă, *J. Am. Chem. Soc.* **2012**, *134*, 12932 – 12935.
[73] S. S. Park, E. R. Hontz, L. Sun, C. H. Hendon, A. Walsh, T. Van Voorhis, M. Dincă, *J. Am. Chem. Soc.* **2015**, *137*, 1774 – 1777.
[74] J. Mei, Z. Bao, *Chem. Mater.* **2014**, *26*, 604 – 615.
[75] T. Panda, R. Banerjee, *Proc. Natl. Acad. Sci. India Sect. A* **2014**, *84*, 331 – 336.
[76] E. L. Spitler, W. R. Dichtel, *Nat. Chem.* **2010**, *2*, 672 – 677.
[77] M. Dogru, A. Sonnauer, A. Gavryushin, P. Knochel, T. Bein, *Chem. Commun.* **2011**, *47*, 1707.
[78] J. Guo, Y. Xu, S. Jin, L. Chen, T. Kaji, Y. Honsho, M. A. Addicoat, J. Kim, A. Saeki, H. Ihee et al., *Nat. Commun.* **2013**, *4*, 1 – 8.
[79] J. W. Colson, W. R. Dichtel, *Nat. Chem.* **2013**, *5*, 453 – 465.
[80] R. Gutzler, D. F. Perepichka, *J. Am. Chem. Soc.* **2013**, *135*, 16585 – 16594.
[81] P. Chaudhuri, C. N. Verani, E. Bill, E. Bothe, T. Weyhermüller, K. Wieghardt, *J. Am. Chem. Soc.* **2001**, *123*, 2213 – 2223.
[82] M. Hmadeh, Z. Lu, Z. Liu, F. Gándara, H. Furukawa, S. Wan, V. Augustyn, R. Chang, L. Liao, F. Zhou et al., *Chem. Mater.* **2012**, *24*, 3511 – 3513.
[83] T. Kambe, R. Sakamoto, K. Hoshiko, K. Takada, M. Miyachi, J.-H. Ryu, S. Sasaki, J. Kim, K. Nakazato, M. Takata et al., *J. Am. Chem. Soc.* **2013**, *135*, 2462 – 2465.
[84] T. Kambe, R. Sakamoto, T. Kusamoto, T. Pal, N. Fukui, K. Hoshiko, T. Shimojima, Z. Wang, T. Hirahara, K. Ishizaka et al., *J. Am. Chem. Soc.* **2014**, *136*, 14357 – 14360.
[85] T. Pal, T. Kambe, T. Kusamoto, M. L. Foo, R. Matsuoka, R. Sakamoto, H. Nishihara, *ChemPlusChem* **2015**, *80*, 1255 – 1258.
[86] J. Cui, Z. Xu, *Chem. Commun.* **2014**, *50*, 3986 – 3988.
[87] A. J. Clough, J. W. Yoo, M. H. Mecklenburg, S. C. Marinescu, *J. Am. Chem. Soc.* **2015**, *137*, 118 – 121.
[88] R. Dong, M. Pfeffermann, H. Liang, Z. Zheng, X. Zhu, J. Zhang, X. Feng, *Angew. Chem. Int. Ed.* **2015**, *54*, 12058 – 12063; *Angew. Chem.* **2015**, *127*, 12226 – 12231.
[89] D. Sheberla, L. Sun, M. A. Blood-Forsythe, S. Er, C. R. Wade, C. K. Brozek, A. Aspuru-Guzik, M. Dincă, *J. Am. Chem. Soc.* **2014**, *136*, 8859 – 8862.
[90] M. G. Campbell, D. Sheberla, S. F. Liu, T. M. Swager, M. Dincă, *Angew. Chem. Int. Ed.* **2015**, *54*, 4349 – 4352; *Angew. Chem.* **2015**, *127*, 4423 – 4426.
[91] M. G. Campbell, S. F. Liu, T. M. Swager, M. Dincă, *J. Am. Chem. Soc.* **2015**, *137*, 13780 – 13783.
[92] J. Liu, Q. Sun, *ChemPhysChem* **2015**, *16*, 614 – 620.
[93] Z. F. Wang, N. Su, F. Liu, *Nano Lett.* **2013**, *13*, 2842 – 2845.
[94] B. Zhao, J. Zhang, W. Feng, Y. Yao, Z. Yang, *Phys. Rev. B* **2014**, *90*, 201403 – 201408.
[95] L. E. Darago, M. L. Aubrey, C. J. Yu, M. I. Gonzales, J. R. Long, *J. Am. Chem. Soc.* **2015**, DOI: 10.1021/jacs.5b10385.
[96] D. Chen, H. Xing, Z. Su, C. Wang, *Chem. Commun.* **2016**, DOI: 10.1039/C5CC09065B.
[97] S. R. Ahrenholtz, C. C. Epley, A. J. Morris, *J. Am. Chem. Soc.* **2014**, *136*, 2464 – 2472.
[98] C. R. Wade, M. Li, M. Dincă, *Angew. Chem. Int. Ed.* **2013**, *52*, 13377 – 13381; *Angew. Chem.* **2013**, *125*, 13619 – 13623.
[99] J. Liu, W. Zhou, J. Liu, I. Howard, G. Kilibarda, S. Schlabach, D. Coupry, M. Addicoat, S. Yoneda, Y. Tsutsui et al., *Angew. Chem. Int. Ed.* **2015**, *54*, 7441 – 7445; *Angew. Chem.* **2015**, *127*, 7549 – 7553.
[100] C. H. Hendon, D. Tiana, T. P. Vaid, A. Walsh, *J. Mater. Chem. C* **2013**, *1*, 95 – 100.
[101] K. T. Butler, C. H. Hendon, A. Walsh, *ACS Appl. Mater. Interfaces* **2014**, *6*, 22044 – 22050.

Received: July 6, 2015
Published online: January 8, 2016

